

# Dynamic adsorption of Xe on a fixed-bed adsorber at 77 K

Bin Long<sup>1,2</sup> · Jun-Li Li<sup>1</sup> · Qun-Shu Wang<sup>2</sup> · Shu-Juan Feng<sup>2</sup> · Guo-Qing Zhou<sup>2</sup> · Tian-Cheng Feng<sup>2</sup> · Yan-Jie Tian<sup>2</sup> · Huai-Cheng Ma<sup>2</sup>

Received: 26 May 2016/Revised: 29 October 2016/Accepted: 2 November 2016/Published online: 26 July 2017

© Shanghai Institute of Applied Physics, Chinese Academy of Sciences, Chinese Nuclear Society, Science Press China and Springer Nature Singapore Pte Ltd. 2017

**Abstract** In designing a fixed-bed adsorber, it is vital to understand dynamic adsorption properties of the unit. Temperature is an important effect on adsorbent performance, as the dynamic adsorption coefficients tend to increase with decreasing temperature. To minimize the volume of the fixed-bed adsorber, the dynamic adsorption characteristics of Xe were studied at 77 K by employing a variety of adsorbents under different operational conditions. The carbon molecular sieve performed better than that of activated carbon. Both operational conditions and the presence of gaseous impurities were found to affect the adsorption properties.

**Keywords** Dynamic adsorption · Xe · 77 K · Carbon molecular sieve · Fixed-bed adsorber

## 1 Introduction

Because of their high fission yields, suitable half-lives and low environmental background concentrations, xenon isotopes are important for detection of clandestine nuclear tests and various aspects of radiation safety [1]. Due to their very low environmental concentrations, xenon isotopes are

very difficult to detect unless they are concentrated by separating them from other gaseous atmospheric components. A common method of xenon enrichment and separation is physical adsorption, which is used in international monitoring systems (IMS) and on-site inspection (OSI) equipment of the Comprehensive Nuclear-Test-Ban Treaty Organization (CTBTO), e.g., ARSA [2–4], SPALAX [5], ARIX [6], SAUNA [4, 7], SAUNA-OSI, ARIX 3F [8] and XESPM-II techniques [1]. The adsorption materials used in these systems include carbon-based molecular sieves, granular-activated carbons and zeolite molecular sieves.

Adsorption is an exothermal process, and dynamic adsorption capacity of a fixed-bed adsorber is inversely proportional to its temperature [9, 10]. The dynamic adsorption coefficient of activated carbon for xenon was 2.56 L/g at 276 K and 0.86 L/g at 328 K [9]. Therefore, it is essential to study the properties of Xe on various adsorbents using a cryostat designed to hold the lower bed temperature and minimize the Xe adsorber dimensions. Conveniently obtainable liquid nitrogen (LN<sub>2</sub>), at 77 K, is used to refrigerate gases in the adsorber efficiently and rapidly. In this work, a fixed-bed adsorber at 77 K was used to study the dynamic adsorption coefficients of different adsorbents and the effects of various operation conditions.

## 2 Theory

According to the adsorption equilibrium theory, dynamic adsorption coefficients can be calculated from the breakthrough curves [10–14]:

$$k_{dB} = Ft_{0.05}/m, \quad (1)$$

This work was supported by the National Natural Science Foundation of China (No. 11405134).

✉ Jun-Li Li  
lijunli@mail.tsinghua.edu.cn

<sup>1</sup> Key Laboratory of Particle and Radiation Imaging of Ministry of Education, Department of Engineering Physics, Tsinghua University, Beijing 100084, China

<sup>2</sup> Northwest Institute of Nuclear Technology, Xi'an 710024, China

$$k_d = Ft_{0.5}/m, \quad (2)$$

where  $k_{dB}$  is the breakthrough dynamic adsorption coefficient,  $k_d$  is the dynamic adsorption coefficient,  $m$  is the adsorbent mass,  $t_{0.05}$  is the breakthrough time,  $t_{0.5}$  is the equilibrium time, and  $F$  is flow rate of outlet gas. The adsorption quantity can be calculated by

$$q = Ft_{0.5}C_0/m = k_dC_0, \quad (3)$$

where  $C_0$  is the equilibrium concentration of Xe in the inlet gas.

The length of unused bed (LUB) to optimize the packed bed length can be approximated by

$$\text{LUB} = (1 - t_{0.05}/t_{0.5})h, \quad (4)$$

where  $h$  is the actual length of the packed bed.

The specific adsorption volume  $V_x$  can be calculated by Eq. (5), where  $V_c$  is the inner volume of the adsorber.

$$V_x = Ft_x/V_c. \quad (5)$$

Zhou Chongyang [15] improved the Wheeler–Jonas equation [11] for convenient calculation of the overall adsorption rate constant ( $k_v$ ) for analysis of the dynamic effect.

$$\begin{aligned} \frac{t_{0.05}}{t_{0.5}} &= 1 - \frac{F}{V_c \times k_v} \ln \left( \frac{C_0 - 0.05C_0}{0.05C_0} \right) \\ &= 1 - 2.944 \times \frac{F}{V_c \times k_v}. \end{aligned} \quad (6)$$

### 3 Experimental

#### 3.1 Experimental apparatus

The test apparatus for dynamic adsorption experiments is shown schematically in Fig. 1.  $N_2$  and Xe were used as the carrier gas and adsorbate, respectively, while the

impurity gas included  $CO_2$ , CO and water vapor. The pressure sensor, dew point meter and flow meter were used to measure inlet and outlet pressures, dew point and flow rate, respectively. A gas chromatograph (GC) was used to measure the concentrations of Xe,  $CO_2$  and CO.

The experiment procedures are as follows. The  $N_2$  and Xe gases were pressurized initially at 0.4 MPa using their respective regulators. The mass flow controllers were adjusted to obtain desired Xe concentration and gas flow rates so that the gases could be mixed adequately and homogeneously. The gas pressure was then adjusted using the adjustable valves at the bed inlet, after which Xe concentration of the inlet gas was determined using the GC (the gas circuit denoted by the dotted line in Fig. 1), employing a 13XHP molecular sieve column to remove water vapor and  $CO_2$  before these species condensed inside the packed bed at low temperature. The pre-cooling column and the fixed-bed adsorber were placed in a thermostat filled with  $LN_2$  at 77 K. Various fixed-bed adsorbents were used, which were made of cylindrical copper tubes and filled with different adsorbents (hereinafter referred to as the adsorption columns). After the effluent gas from the buffer tank achieved a pressure sufficiently stable for the GC analysis, the Xe concentration in the effluent was monitored at 5-min intervals. At the end of gas circuit, the flow rate was determined with the soap-film flow meter, and dew point was monitored by dew point meters near Valve 4 and the buffer tank.

The effects of gaseous impurities on Xe adsorption were determined by switching on the pressurized containers of  $CO_2$  and CO or the water vapor generator. This was accomplished by closing Valves 3, 4 and 6 and opening Valve 5.

#### 3.2 Adsorbents

The adsorbents included carbon molecular sieves and granular coconut shell-activated carbon. The 01-CMS,

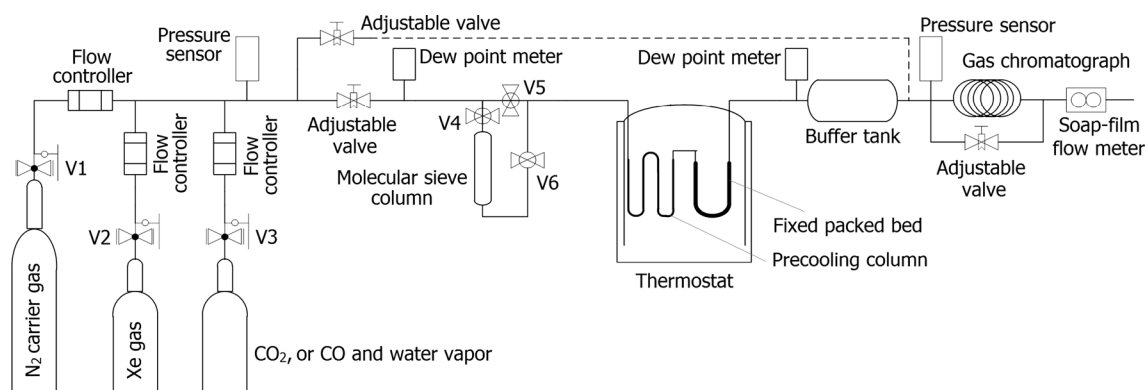


**Fig. 1** Test apparatus for dynamic adsorption experiments

501CMS and 601CMS were produced by Shanghai Institute of Fine Chemicals, China. TJ-CMS was manufactured by Tianjin Chemical Reagent Co., Ltd., China. NM-GAC was produced by Zhongsen Activated Carbon Co., Ltd., Inner Mongolia, China. HN-GAC was procured from Shuangxinlong Industrial and Trading Co., Ltd., Hainan Province, China. Properties of the adsorption columns and adsorbents are summarized in Table 1, where  $S_{\text{BET}}$  is the BET specific surface area;  $V_t$  is the total pore volume;  $S_{\text{micro}}$  and  $V_{\text{micro}}$  are the specific surface area and the pore volume for micropores calculated with the t-plot method, respectively;  $L_{\text{micro}}$  is the diameter of micropores calculated with the D-R model; and  $E_0$  is the characteristic energy of adsorption.

### 3.3 Gas chromatography

A HP6890 GC equipped with a thermal conductivity detector (TCD) was used to analyze the gas concentrations. The operational conditions are presented in Table 2.

## 4 Results and discussion

### 4.1 Dynamic adsorption of Xe on different adsorbents

Characteristics of dynamic Xe adsorption on different adsorbents are determined using the gas circuit in Fig. 1. The results are given in Table 3. Based on the specific Xe desorption volume of 8 for activated carbon or a carbon molecular sieve [15], and purities of Xe adsorbed by different adsorbents, the overall adsorption rate constant ( $k_v$ ) could be calculated by Eq. (6).

Typical breakthrough curve of TJ-CMS at 77 K is shown in Fig. 2a. The curve is S-shaped, and multilayer adsorption can be seen clearly. The Xe boiling point is 165 K, while  $\text{LN}_2$  is at 77 K, and xenon may be liquefied. The kinetic energy of xenon molecules then decreases, and the inner pressure of the adsorber increases. This increases

the contact time between the adsorbent pore surfaces and xenon molecules, and xenon in liquid state is captured by carbon adsorbents. Meanwhile, because of the large specific surface area of carbon adsorbents, more adsorption sites can be provided for xenon. These factors cause advantageous conditions for larger adsorption capacity.

From Table 3,  $k_{\text{dB}}$  and  $k_d$  values of the carbon molecular sieves are higher than those of the activated carbon. For carbon molecular sieves, the maximum  $k_{\text{dB}}$  and  $k_d$  values for the TJ-CMS are 385.5 and 1417 L/g, respectively, and the purity of Xe is 82%, which is  $2.1 \times 10^4$  times the inlet concentration of Xe. For activated carbons, the  $k_{\text{dB}}$  of the NM-GAC is greater than that of the HN-GAC, though its  $k_d$  is lower. The LUB of 01-CMS, TJ-CMS and 501CMS is approximately 14 cm. The  $k_d$  of NM-GAC is 547.4 L/g at 77 K, which is over 200 times the  $k_d$  at 276 K [9]. It is apparent that multilayer adsorption occurs on the CMS and activated carbons at 77 K, leading to the much higher adsorption capacities of the materials. From Table 1, TJ-CMS has a larger BET area and micropores surface area, with narrower micropore diameter than those of other adsorbents, which means larger adsorption capacity and better adsorption selectivity for Xe. The  $k_{\text{dB}}$  values are important, and they are commonly used to design the first stage of an adsorption column to ensure high recovery of Xe.

The results indicate that the minimum  $k_v$  is  $5010 \text{ min}^{-1}$  (TJ-CMS), and the maximum  $k_v$  is  $9034 \text{ min}^{-1}$  (NM-GAC). The  $k_v$  varies with the gas diffusion rate, which depends on the volume proportion of macropores and medium pores.

For confirming the multilayer adsorption of Xe on carbon adsorbents, the adsorption equilibrium isotherm of TJ-CMS was measured at 77 K with nitrogen as the analysis gas by Autosorb iQ Station (Quantachrome Instruments, USA). The isotherm of TJ-CMS is shown in Fig. 2b. According to the classification of IUPAC [16], the adsorption isotherm of TJ-CMS at 77 K is I-type, which agrees well with the multisite Langmuir model. Micropore filling occurs at smaller  $P/P_0$  ratios. Due to the existence of

**Table 1** Properties of the adsorbents (refer to the text for the acronyms and subscripts)

Types	Index	Mass (g)	$S_{\text{BET}}$ ( $\text{m}^2/\text{g}$ )	$V_t$ ( $\text{cm}^3/\text{g}$ )	$S_{\text{micro}}$ ( $\text{m}^2/\text{g}$ )	$V_{\text{micro}}$ ( $\text{cm}^3/\text{g}$ )	$L_{\text{micro}}$ (nm)	$E_0$ (kJ/mol)
Carbon molecular sieve	01-CMS	0.20	1049	1.04	942	0.43	1.18	20.6
	TJ-CMS	0.26	1129	0.50	1047	0.41	0.68	27.3
	501CMS	0.20	1023	0.99	890	0.41	1.17	20.6
	601CMS	0.19	1002	0.97	861	0.40	1.20	20.4
Activated carbon	NM-GAC	0.18	1038	0.65	784	0.34	0.93	23.0
	HN-GAC	0.22	874	0.47	887	0.42	1.19	20.5

Adsorption column,  $\phi$  3.175 mm  $\times$  200 mm, inner diameter, 1.59 mm; adsorbent mesh, 0.25–0.38 mm

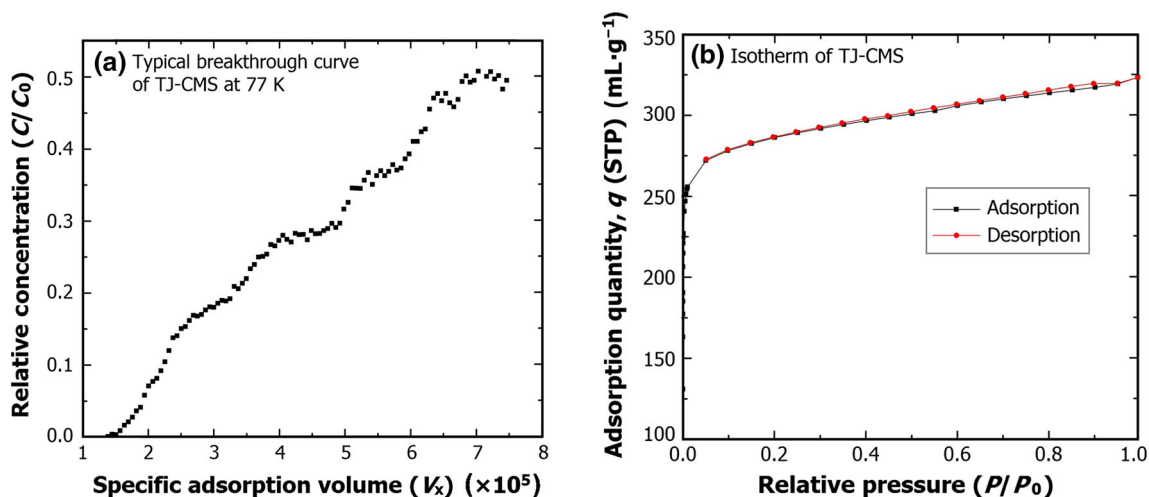
**Table 2** GC operational conditions

Analysis objects	Oven temperature (°C)	Types of column	Column flow (mL/min)	Ref flow (mL/min)
CO <sub>2</sub> , Xe	80	Porapak Q	10	26
CO, Xe	100	5A	12	33

Detector temperature, 205 °C; column size,  $\Phi$  1/8 in  $\times$  2 m; column mesh, 60–80; makeup flow, 2 mL/min

**Table 3** Dynamic adsorption characteristics of Xe at 77 K

Adsorbents	$C_0$ ( $\times 10^{-6}$ V/V)	$F$ (mL/min)	$t_{0.05}$ (min)	$t_{0.5}$ (min)	$k_{dB}$ (L/g)	$k_d$ (L/g)	$q$ (mL/g)	LUB (cm)	Purity (%)	$k_v$ (min <sup>-1</sup> )
01-CMS	39.07	515	142	482	365.8	1242	48.51	14.1	75.4	5424
TJ-CMS	39.07	491	157	577	385.5	1417	55.35	14.6	82.0	5010
501CMS	38.64	510	146	551	372.2	1405	54.27	14.7	77.4	5151
601CMS	43.04	508	135	275	360.6	735	31.62	10.2	65.5	7411
NM-GAC	38.64	547	110	200	301.1	547	21.15	9.0	54.6	9034
HN-GAC	38.64	529	62	247	164.1	654	25.26	15.0	63.7	5249

**Fig. 2** (Color online) Breakthrough curve (a) and adsorption isotherm (b) of TJ-CMS at 77 K

macropores and medium pores, multilayer adsorption takes place as the relative pressure  $P/P_0$  increases; while as  $P/P_0$  increases, the phenomenon of capillary condensation appears. Both multilayer adsorption and capillary condensation are useful for enhancing the adsorption. However, when the degree of capillary condensation becomes too large, the adsorbed gas may be frozen, and it may even jam the fixed-bed adsorber.

#### 4.2 The Xe concentration effects

The Xe concentration affects the dynamic adsorption performance. The coefficients of Xe dynamic adsorption on TJ-CMS tested at different Xe concentrations are shown in Fig. 3a. The  $k_{dB}$  and  $k_d$  decrease with increasing Xe

concentration until  $k_d = 117 \times 10^{-6}$  V/V, where they begin to increase. Polynomial fittings were performed between  $\ln k_{dB}$  or  $\ln k_d$  and  $\ln C_0$ , and the results are shown in Eqs. (7) and (8).

$$\ln k_{dB} = 0.545(\ln C_0)^2 - 4.845 \ln C_0 + 16.17, R^2 = 0.930, \quad (7)$$

$$\ln k_d = 0.226(\ln C_0)^2 - 2.199 \ln C_0 + 12.30, R^2 = 0.989. \quad (8)$$

In Fig. 3b, the adsorbed quantity increases linearly with the Xe concentration. As the concentration increases, the gases in the adsorption column tend to liquefy at 77 K, and capillary condensation occurs. Also, because of the large specific area of TJ-CMS, sufficient adsorption sites can be

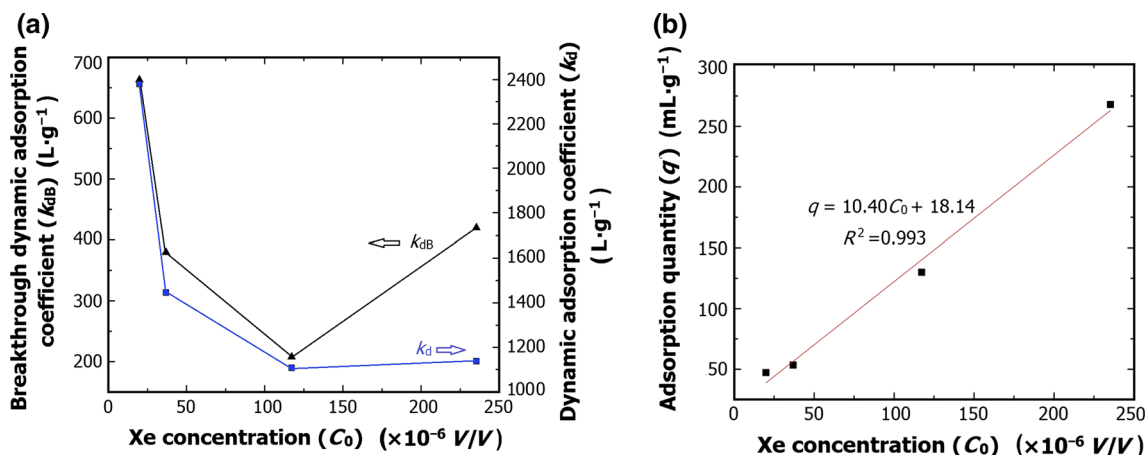


**Fig. 3** (Color online) Effects of Xe concentration on  $k_{dB}$  and  $k_d$  of TJ-CMS (a) and the fitted line (b) between Xe concentration ( $C_0$ ) and adsorbed amount ( $q$ ) of Xe on TJ-CMS, at 492–519 mL/min of low rate and  $19.9 \times 10^{-6}$ – $235 \times 10^{-6}$  V/V of Xe concentration

provided, and the liquefaction of Xe at 77 K can be captured easily by micropores of the TJ-CMS adsorbent. According to the gas–solid adsorption theory, the equilibrium adsorption amount of gas adsorbent increases as the partial pressure of the key gas component increases. The increasing Xe concentration is equivalent to the increasing partial pressure of Xe. Therefore, the above factors result in the decreased adsorption coefficient and the increased adsorption amount.

The  $k_v$  values listed in Table 4 indicate that  $k_v$  varied slightly with the Xe concentration.

### 4.3 The gas flow rate effects

Using the TJ-CMS carbon molecular sieves, the effects of gas flow rate on the dynamic adsorption of Xe at 77 K were studied under flow rate of 509–1348 mL/min and Xe concentrations of  $37 \times 10^{-6}$ – $45 \times 10^{-6}$  V/V. As shown in Fig. 4, the  $k_{dB}$  and  $k_d$  decrease with increasing flow rate, from  $k_{dB} = 380$  L/g and  $k_d = 1500$  L/g at the gas flow rate of 509 mL/min to  $k_{dB} = 150$  L/g and  $k_d = 450$  L/g at the gas flow rate of 1348 mL/min. Because the linear velocity of gas increases with the flow rate, the gas flowing through the adsorption column may be not adequately cooled, hence the increase in thermal motion of the gas molecules.

**Table 4** Overall adsorption rate constant ( $k_v$ ) at different Xe concentrations

$C_0$ ( $\times 10^{-6}$ V/V)	$F$ (mL/min)	$t_{0.05}$ (min)	$t_{0.5}$ (min)	$k_v$ ( $\text{min}^{-1}$ )
20	519	332	1192	5346
37	509	194	739	5124
117	515	105	560	4704
235	492	222	602	5783

Under these conditions, flow rate makes a great difference in the dynamic adsorption performance.

As shown in Fig. 4b,  $k_v$  increases with the gas flow rate. This agrees with the results in Refs. [15, 17]. As the Xe diffusion rate increases with the gas flow rate, the contact between Xe molecules and the adsorption interfaces of adsorbents becomes easier, and contact time shortens. Therefore,  $k_v$  increases with the flow rate, but the adsorption capacity decreases.

### 4.4 The inlet pressure effects

The inlet pressure effects on the dynamic adsorption of Xe at 77 K were assessed at the gas flow rates of 565–573 mL/min and Xe concentration of  $33 \times 10^{-6}$ – $45 \times 10^{-6}$  V/V. As shown in Fig. 5, the  $k_{dB}$  and  $k_d$  increase with the inlet pressure, agreeing with reports in Ref. [10]. The inlet pressure is the most important factor for designing adsorption columns and gas circuits. The  $k_v$  data in Table 5 indicate that  $k_v$  changes slightly with the inlet pressure.

### 4.5 The inner diameter effects

The adsorption capacity of adsorbents is known to decrease with increasing linear velocity of the gas. A common way of reducing the effects of a high linear velocity is to increase the pre-column pressure and inner diameter of the adsorption column. Therefore, we studied inner diameter effects of the adsorption column on Xe dynamic adsorption over the carbon molecular sieve TJ-CMS at 77 K. The results are summarized in Table 6. The linear velocities in each test were about the same. While the  $k_{dB}$  data obtained at the inner diameters of 1.6 and 4.2 mm were similar (283 and 257 L/g), the  $k_{dB}$  became

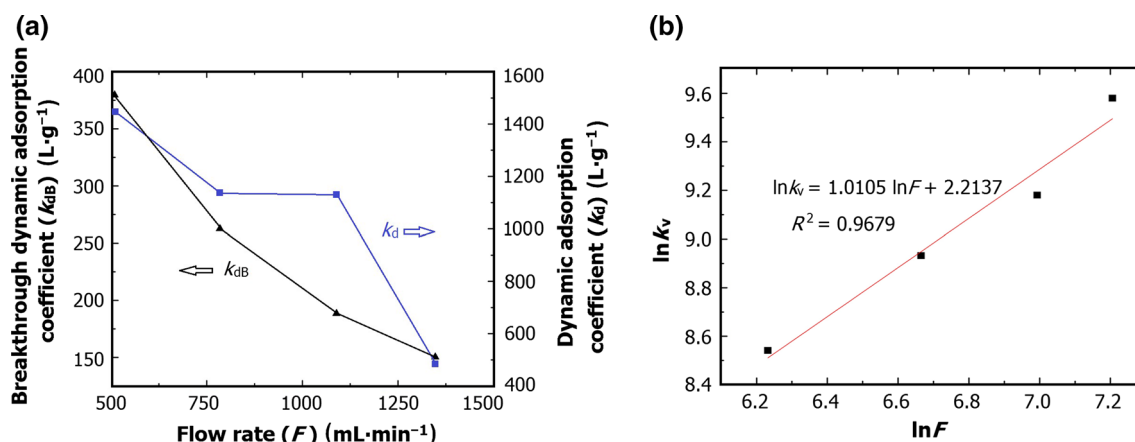


**Fig. 4** (Color online)  $k_{dB}$  and  $k_d$  (a) and  $k_v$  (b), as function of the flow rate, at 509–1348 mL/min of flow rate and  $37 \times 10^{-6}$ – $45 \times 10^{-6}$  V/V of Xe concentration

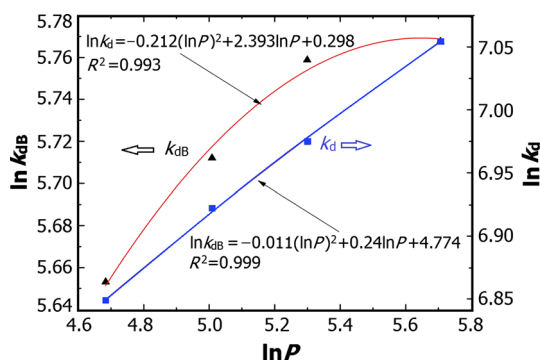


**Fig. 5** (Color online)  $k_{dB}$  and  $k_d$  as function of the inlet pressure ( $P$ ), at flow rate of 565–573 mL/min and Xe concentration of  $33 \times 10^{-6}$ – $45 \times 10^{-6}$  V/V

**Table 5** Overall adsorption rate constant ( $k_v$ ) at different inlet pressures

$P$ (kPa)	$F$ (mL/min)	$t_{0.05}$ (min)	$t_{0.5}$ (min)	$k_v$ ( $\text{min}^{-1}$ )
108	565	130	440	5960
150	565	136	486	5823
200	550	144	539	5578
301	573	145	525	5883

1215 L/g at the inner diameter of 6.8 mm, when the inlet pressure increased to 401 kPa from a few hundred kPa.

#### 4.6 The CO<sub>2</sub> concentration effects

The CO<sub>2</sub> concentration effects on the dynamic adsorption of Xe were examined on TJ-CMS at 77 K, under the gas flow rates of 518–576 mL/min and Xe concentration of  $37 \times 10^{-6}$ – $40 \times 10^{-6}$  V/V. As shown in Fig. 6a, the  $k_{dB}$  value on TJ-CMS decreases with the CO<sub>2</sub> concentration and then increases. Because of the competitive adsorption, the existence of CO<sub>2</sub> results in the decrease in xenon adsorption capacity. The sublimation temperatures of CO<sub>2</sub> and Xe are 194 and 165 K, respectively, so CO<sub>2</sub> can be liquefied easier than xenon, and the extent of gas liquefaction inside the adsorption column increases with the CO<sub>2</sub> concentration. The extent of capillary condensation is very high during the adsorption process of CO<sub>2</sub>, and the micropores used to adsorb Xe are occupied by CO<sub>2</sub> molecules so that the micropores volumes which are fit for the adsorption of xenon become smaller. The inlet pressure versus the ventilation duration at  $2722 \times 10^{-6}$  V/V of CO<sub>2</sub> is plotted in Fig. 6b. It shows that the inlet pressure would increase to some degree due to CO<sub>2</sub> liquefaction. As the

**Table 6** Effects of adsorption column inner diameter on dynamic adsorption

Flow rate (mL/min)	Linear velocity (cm/s)	Inner diameter of adsorption column (mm)	Inlet pressure (kPa)	$k_{dB}$ (L/g)
565	476	1.6	108	283
3755	452	4.2	193	257
10,804	496	6.8	401	1215

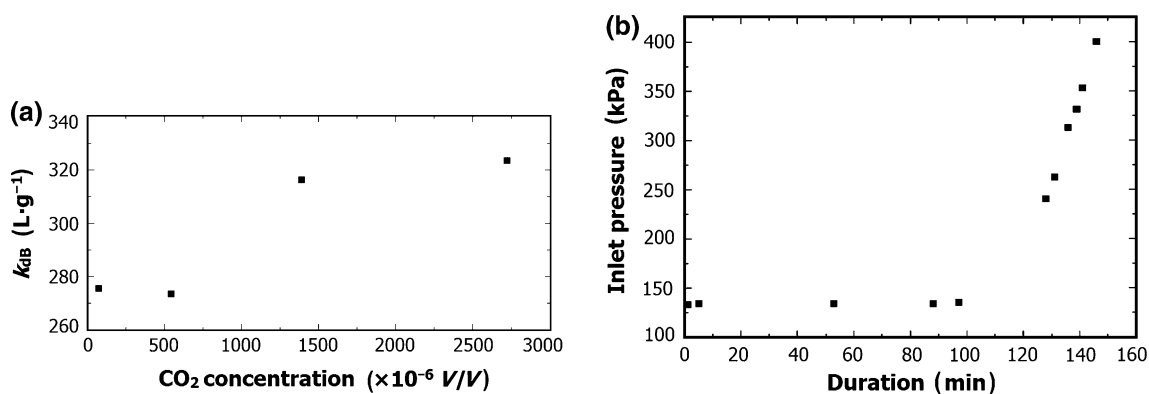


**Fig. 6** Dynamic adsorption of Xe as a function of CO<sub>2</sub> concentration (a) and the pre-column pressure versus ventilation duration (b) at CO<sub>2</sub> concentration of  $2722 \times 10^{-6}$  V/V, flow rate of 518–576 mL/min and Xe concentration of  $37 \times 10^{-6}$ – $40 \times 10^{-6}$  V/V

CO<sub>2</sub> concentration increases, the flow rate reduces owing to CO<sub>2</sub> condensation. So, CO<sub>2</sub> must be removed prior to Xe adsorption.

#### 4.7 The CO concentration effects

The CO concentration effects on the dynamic adsorption of Xe were assessed with TJ-CMS at 77 K, under the gas flow rate of 509–554 mL/min, Xe concentration of  $35 \times 10^{-6}$ – $37 \times 10^{-6}$  V/V and inlet pressure of 114–129 kPa. The data are summarized in Table 7. The  $k_{dB}$  and  $k_d$  decrease with increasing CO concentration. Therefore, CO must also be removed before Xe adsorption.

#### 4.8 The water vapor concentration effects

According to Ref. [1], water vapor tends to reduce the adsorption of Xe, and it may also form ice plugs within the adsorption column. The water vapor effects on the dynamic adsorption of Xe were therefore analyzed using the carbon molecular sieve TJ-CMS at 77 K. The  $k_{dB}$  values are 415.8, 256.5 and 245.0 L/g at moisture contents of  $1 \times 10^{-6}$ ,  $76 \times 10^{-6}$  and  $553 \times 10^{-6}$  V/V, respectively, at Xe concentrations of  $36.6$ – $38.5 \times 10^{-6}$  V/V and flow rates of 533–575 mL/min. The  $k_{dB}$  values over TJ-CMS decrease with increasing water vapor concentration. Moreover, at

higher concentrations, the water vapor readily condenses and freezes in the adsorption column, creating a blockage. Then, water vapor must be removed before Xe adsorption.

#### 4.9 Uncertainty estimation

The sources of uncertainties of the dynamic adsorption coefficients of Xe include the uncertainty of the concentration of standard gases (Xe, CO<sub>2</sub> and CO; <2%), the uncertainty of the values of flow rates with the flow rate controller (<2%), the uncertainty of the test values of the pressure sensor (<2%) and the uncertainty of the peak area of GC (<3%). The above entries are independent from each other, and the combined standard uncertainty of the dynamic adsorption coefficient is less than 10% ( $k = 2$ ).

### 5 Conclusion

It is necessary to study the dynamic adsorption properties of a gas before designing a fixed-bed adsorber. In this paper, the dynamic adsorption characteristics of Xe on various fixed-bed adsorbents were studied at 77 K, including the dynamic adsorption coefficients of different adsorbents and the effects of a variety of operational conditions. The dynamic adsorption performances of carbon molecular sieves are very attractive because they allow us to minimize the adsorption volume at ultra-low temperatures. The TJ-CMS generated the highest  $k_{dB}$  and  $k_d$  values among the adsorbents assessed. And increasing the concentrations of CO<sub>2</sub>, CO and water vapor reduced the adsorption of Xe because these gases tended to liquefy and even freeze in the adsorption column, resulting in pipeline blockage. Therefore, the removal of gaseous impurities of CO<sub>2</sub> and water vapor with zeolite molecular sieves must be considered because of their excellent adsorption capacities and higher characteristic adsorption energies for polar molecules. These results can be seen as one of the

**Table 7** Effects of CO concentration on dynamic adsorption

CO concentration (× 10 <sup>-6</sup> V/V)	<i>t</i> <sub>0.05</sub> (min)	<i>t</i> <sub>0.5</sub> (min)	<i>k</i> <sub>dB</sub> (L/g)	<i>k</i> <sub>d</sub> (L/g)
0	157	577	385.5	1417
100	145	560	302	1168
200	130	500	274	1054
1000	128	438	273	953

Flow rate, 509–554 mL/min; Xe concentration,  $35 \times 10^{-6}$ – $37 \times 10^{-6}$  V/V; inlet pressure, 114–129 kPa

important criteria for designing a radioxenon separation and enrichment system, and they provide a reference for other fields of xenon separation.

**Acknowledgements** The authors are wishing to acknowledge Dr. Chong-yang Zhou for his creative suggestions.

## References

1. C.Y. Zhou, G.Q. Zhou, S.J. Feng et al., The determination of trace amounts of natural  $^{133}\text{Xe}$  in gas under high radon activity concentration levels. *J. Environ. Radioact.* **122**, 9–15 (2013). doi:[10.1016/j.jenvrad.2013.02.006](https://doi.org/10.1016/j.jenvrad.2013.02.006)
2. J.I. McIntyre, K.H. Abel, T.W. Bowyer et al., Measurements of ambient radioxenon levels using the automated radioxenon sampler-analyzer (ARSA). *J. Radioanal. Nucl. Chem.* **248**(3), 629–635 (2001). doi:[10.1023/A:1010672107749](https://doi.org/10.1023/A:1010672107749)
3. T.W. Bowyer, C. Schlosser, K.H. Abel et al., Detection and analysis of xenon isotopes for the comprehensive nuclear-test-ban treaty international monitoring system. *J. Environ. Radioact.* **59**, 139–151 (2002). doi:[10.1016/S0265-931X\(01\)00042-X](https://doi.org/10.1016/S0265-931X(01)00042-X)
4. M. Auer, T. Kumberg, H. Sartorius et al., Ten years of development of equipment for measurement of atmospheric radioactive xenon for the verification of the CTBT. *Pure Appl. Geophys.* **167**, 471–486 (2010). doi:[10.1007/s00024-009-0027-y](https://doi.org/10.1007/s00024-009-0027-y)
5. J.P. Fontaine, F. Pointurier, X. Blanchard et al., Atmospheric xenon radioactive isotope monitoring. *J. Environ. Radioact.* **72**, 129–135 (2004). doi:[10.1016/S0265-931X\(03\)00194-2](https://doi.org/10.1016/S0265-931X(03)00194-2)
6. Y.V. Dubasov, Y.S. Popov, V.V. Prelovskii et al., The APIKC-01 automatic facility for measuring concentrations of radioactive xenon isotopes in the atmosphere. *Instrum. Exp. Tech.* **3**, 108–114 (2005). doi:[10.1007/s10786-005-0065-3](https://doi.org/10.1007/s10786-005-0065-3)
7. A. Ringbom, T. Larson, A. Axelsson et al., SAUNA—a system for automatic sampling, processing, and analysis of radioactive xenon. *Nucl. Instrum. Methods A* **508**(3), 542–553 (2003). doi:[10.1016/S0168-9002\(03\)01657-7](https://doi.org/10.1016/S0168-9002(03)01657-7)
8. V.V. Prelovskii, N.M. Kazarinov, A.Y. Donets et al., The ARIX-03F mobile semiautomatic facility for measuring low concentrations of radioactive xenon isotopes in air and subsoil gas. *Instrum. Exp. Tech.* **50**, 393–397 (2007). doi:[10.1134/S0020441207030165](https://doi.org/10.1134/S0020441207030165)
9. C.Y. Zhou, S.J. Feng, G.Q. Zhou et al., The behavior of xenon dynamic adsorption on granular activated carbon packed bed adsorber. *J. Radioanal. Nucl. Chem.* **287**, 609–616 (2011). doi:[10.1007/s10967-010-0878-9](https://doi.org/10.1007/s10967-010-0878-9)
10. G.O. Wood, A review of the effects of covapors on adsorption rate coefficients of organic vapors adsorbed onto activated carbon from flowing gases. *Carbon* **40**, 685–694 (2002). doi:[10.1016/S0008-6223\(01\)00185-3](https://doi.org/10.1016/S0008-6223(01)00185-3)
11. G.O. Wood, Quantification and application of skew of breakthrough curves for gases and vapors eluting from activated carbon beds. *Carbon* **40**, 1883–1890 (2002). doi:[10.1016/S0008-6223\(02\)00031-3](https://doi.org/10.1016/S0008-6223(02)00031-3)
12. Y. Nakayama, H. Nagao, I. Mochida et al., Adsorption of radon on active carbon. *Carbon* **32**, 1544–1547 (1994). doi:[10.1016/0008-6223\(94\)90154-6](https://doi.org/10.1016/0008-6223(94)90154-6)
13. D.P. Siegworth, C.K. Neulander, R.T. Pao et al., Measurement of dynamic adsorption coefficients for noble gases on activated carbon. In *Proceedings of the 12th AEC Air Cleaning Conference, San Jose, CA*, ed. by M.W. First. National Technical Information Service, Springfield, VA, (1972), pp. 28–47. **(to be published)**
14. R.E. Adams, W.E. Browning, R.D. Ackley, Containment of radioactive fission gases by dynamic adsorption. *Ind. Eng. Chem.* **51**, 1467–1470 (1959). doi:[10.1021/ie50600a032](https://doi.org/10.1021/ie50600a032)
15. C.Y. Zhou, Study on the technology of Xenon enrichment and separation from atmosphere and its application in nuclear inspection. Ph. D. Thesis, Tsinghua University, 2011 **(in Chinese)**
16. S.W. Sing, D.H. Everett, R.A.W. Haul et al., Reporting physisorption data for gas/solid systems with special reference to the determination of surface area and porosity. *Pure Appl. Chem.* **57**(4), 603–619 (1985). doi:[10.1351/pac198557040603](https://doi.org/10.1351/pac198557040603)
17. C.Y. Zhou, S.J. Feng, G.Q. Zhou et al., A simple method for calculating the overall adsorption rate constant in the Wheeler–Jonas equation. *Adsorpt. Sci. Technol.* **29**(1), 71–82 (2011). doi:[10.1260/0263-6174.29.1.71](https://doi.org/10.1260/0263-6174.29.1.71)